Sodium silicate corrosion inhibition behaviour for carbon steel in a dynamic salt water environment

E. De Ketelaere[a], D.Moed[b], M. Vanoppen[c], A. R.D. Verliefde[c], K.Verbeken[a,*], T.Depover[a,*]

[a]Ghent University, Department of Materials, Textiles and Chemical Engineering, Research Group Sustainable Materials Science, Zwijnaarde, Belgium.
[b]Evides Industriewater, Rotterdam, The Netherlands.
[c]Ghent University, Department of Green Chemistry and Technology, Research Group Particle and Interfacial Technology, Ghent, Belgium.

2022

Abstract

This work investigates the sustainable green corrosion inhibitor sodium silicate (SS) in inhibition efficiency (IE) and mechanism for carbon steel in a dynamic 3wt.% NaCl environment. Electrochemical impedance spectroscopy and potentiodynamic scans are performed within a rotating cylinder electrode setup at variable conditions. Increasing SS dosage ($\leq 10mM$) under constant laminar flow results in higher IE (up to 99.8%), linked to replacement of water by silicate species, followed by more structured film formation at the steel surface. Increasing flow rate results in maximum IE at intermediate flow rate, linked to faster transport of silicate and cathodic species to the steel surface and more mechanical removal of the film.

Keywords

A. carbon steel
B. EIS
B. polarization
C. neutral inhibition
C. oxide coatings

* corresponding authors.
E-mail adresses: Elias.Deketelaere@UGent.be (E. De Ketelaere), D.Moed@Evides.nl (D. Moed), Arne.Verliefde@UGent.be (A.R.D. Verliefde), Kim.Verbeken@UGent.be (K. Verbeken), Tom.Depover@UGent.be (T. Depover)

1 Introduction

Metal corrosion is often a weak link in the reliability of industrial cooling water cycles. Degradation of pipe material or critical components in these streams can cause process related issues like disturbances in the water flow, leakage and deposition of corrosion products on heat-exchanger components, possibly resulting in a lowered efficiency [1]. Furthermore, metal dissolution elevates the concentration of metal species in the water and eventually this dissolved metal ends up in surface waters during a periodic blow-down. There are several strategies to limit corrosion in cooling water systems, including the modification of the utilized metal equipment (e.g. coating, plating, surface treatment or change in alloy composition), protecting the metal by applying anodic or cathodic protection, or altering the aqueous environment [2]. Modifications in the environment can be done by changing operational parameters like temperature, flow rate and pH, but can also include removing aggressive species (e.g. chloride) or the addition of corrosion inhibiting chemicals.

Due to their good inhibiting performance, in the past, chromate- and nitrate-based corrosion inhibitors were used predominantly to prevent corrosion in industrial installations. As it stands, these substances can no longer be used because of their inherent toxicity and environmental restrictions as a result [3–5]. This discovery urged the development of new competitive corrosion inhibitors with non-toxicity, cost and eco-friendliness as primary objectives [6–9]. Promising candidates for these sustainable inhibitors include phosphonates, rare-earth metal compounds, silicates, plant extract-based inhibitors and organic compounds containing electron rich hetero-atoms like O, N, P and S [2–4, 10–13]. Here, it should be mentioned that inorganic phosphorous (phosphate-based inhibitors) compounds, despite their corrosion inhibiting performance, should be avoided as their environmental impact (i.e. eutrophication) cannot be ignored [5, 14–17]. Frequently used phosphonate compounds, on the other hand, would only cause eutrophication over a longer period of time [3]. However, as phosphonates are poorly biodegradable by design, usage of these species are noticed in its concentration in the surface water. As a consequence, phosphonates are being limited in their use due to their harmful properties.

An especially interesting group of inhibitors can be found within the silicate based compounds. Sodium silicate (SS) is produced in several forms, which can be distinguished based on their weight ratio of SiO_2/Na_2O. In practice, grades with a SiO_2/Na_2O-ratio varying from 1 to 3.8 are produced, with most commercial products having a ratio of 3.22 [11]. These silicate based compounds are especially interesting due to their non-toxic nature and good availability. [5,18] Sodium silicates have been used as a corrosion inhibitor over the last century, with the first observations on the protective silicate layers dating back to the early 1920's [11, 19]. Some authors [20, 21] found that an iron oxide layer with a layered $Fe_2O_3/FeO/Fe$ structure [20] or a thin $\gamma - Fe_2O_3$ film is responsible for the protective effect of sodium silicate. Other observations also indicated the incorporation of silicate in the protective layer on the tested steel samples [5, 16, 22–29]. In addition to film formation, self-healing properties were also postulated if silica is continuously fed

into the system [11, 30–32]. This means that in case of film damage (e.g. due to erosion or corrosion), the silicate of the surrounding film and in the solution near the steel surface is used to form a new protective film layer where the damage is produced. However, SS is also known to be less effective in systems containing dissolved Mg and Ca and in lower pH aqueous environments (pH<9) [11, 21, 31, 33].

In industrial installations and especially for cooling water cycles, water is often flowing through pipes or components. This means that these hydrodynamic conditions could be an important factor to take into account for conditioning the water within these systems. Previous works indicate that sodium silicate uptake is usually higher in stagnant water conditions, basing their findings on loop tests within piping and weight loss analysis [11,19,34]. However, addition of electrochemical measurements and accurate control of flow regime are absolutely necessary to allow for more than just a qualitative estimate on the influence of hydrodynamic conditions on silica inhibition. Moreover, for steel [35–37] as well as with other materials [36,38], it was found that an increased flow rate influences the rate of mass transfer of species involved with the formation and removal of protective- or oxide films. In a work on aluminium in a boric acid environment [38], potentiodynamic scans (PDS) indicate increased measured corrosion currents and higher corrosion potentials with increased flow rates. With the addition of electrochemical impedance spectroscopy (EIS) measurements a gradual loss in electrical resistance of the oxide film could be identified, which is due to the elevated dissolution of the oxide film at these higher flow rates. On uninhibited steels in neutral (chlorine-rich) environments on the other hand, the formation of different corrosion products can be promoted as a result of a higher oxygen supply at higher flow rates. [35, 36] For some inhibitor mixtures, EIS and PDS measurements were performed at varying electrode rotation speeds, indicating improved inhibition as a result of higher laminar flow rates. [27, 29, 37] In a study on the corrosion inhibition behaviour of sodium silicate on magnesium [31], passive behaviour was noticed in PDS scans upon dosing larger amounts (5-10 mM) of SS. Furthermore, additional EIS measurements as well as morphological studies revealed compacting of the resulting coating. Additionally, the appearance of phase angle peak at low frequencies indicated the formation of an inner layer within the film structure. Similar EIS spectra were obtained in a study concerning steel submerged in a 3.5 wt.% NaCl solution with added SS in combination with modified chitosan-oligosaccharide (MCO). [27] Here, two phase noses were also identified, as well as an increase of both the general impedance modulus and charge transfer resistance with dosage of SS, MCO and MCO-SS blend. This result is linked to the increased corrosion resistance of the steel, resulting from the displacement of water molecules and the combined formation of SS and MCO on the metal surface, with SS blocking the (uninhibited) active sites. A different behaviour was observed in a study [3] on carbon steel in tap water in combination with SS and polyamidoamine dendrimers (PAPAM). Here, only a single capacitive loop was fit to the EIS spectra obtained. However, an increase in charge transfer resistance was observed, related to the formation of a protective film on the steel surface. Furthermore, a replacement of water molecules by inhibitor molecules (i.e. PAPAM and SS) was linked to the gradual decrease in double layer capacitance. Additional AFM measurements, combined with EIS analysis

on these samples showed a clear smoothening of the inhibited surfaces. A co-adsorption of PAPAM and SS was concluded as a probable corrosion mechanism, with the synergistic performance as a result.

Although there is a good amount of research indicating the protective properties of sodium silicate [5, 27, 29, 31, 39, 40], little focus is put on the effect of flow rate on corrosion inhibition by sodium silicate and the underlying mechanism. In order to get a better understanding of the influence of different hydrodynamic conditions on the corrosion inhibition provided by sodium silicate ($Na_2Si_3O_7$), electrochemical measurements are performed under different flow conditions within a controlled environment. Additionally, PDS and EIS measurements in a solution with a varying SS concentration at a constant flow rate are performed and analysed to gain new insights on the silicate film formation mechanism under laminar flow conditions.

2 Materials and Methods

2.1 Materials

The chemical composition of the tested S235JR steel, is given in Table 1. For the dynamic testing of this material, ring-shaped samples are prepared to fit within a rotating cylinder electrode setup (section 2.2) as working electrode. As such, three electrode open circuit potential (OCP) measurements, potentiodynamic scans (PDS) as well as electrochemical impedance spectroscopy (EIS) measurements can be executed. Before each electrochemical measurement, the steel electrode is polished using emery paper until 2000 grade. Afterwards, the samples are cleaned using distilled water and dried. Extreme water conditions are opted for, by using a 3 wt.% NaCl solution as an electrolyte, with a sodium silicate solution ($Na_2Si_3O_7 \cdot xH_2O$) added as corrosion inhibitor. Sodium silicate (SS) is added in concentrations of 0.1, 0.5, 1, 5, 10 and 20 mmol/L, with the solution being mixed for 1h before the measurement.

Table 1: Chemical composition of S235JR steel; Maximum concentrations given in wt.%

C	Mn	P	S	Si	Fe
0.22%	1.60%	0.05%	0.05%	0.05%	balance

2.2 Rotating cylinder electrode (RCE)

The used electrochemical cell is incorporated within a rotating cylinder electrode (RCE) setup, for which a schematic illustration is given in Figure 1). The ring-shaped working electrode is attached to a Gamry RDE710 rotor, which can be programmed to revolve at a preset rotation speed. The rotor itself has an external connection that is later attached to the cable leads of the potentiostat in order to perform PDS (section 2.3) and EIS measurements (section 2.4). During these experiments, the rotation speed is varied between 0.5 and 1 m/s at the metal surface. The electrochemical cell itself has a volume of 1 L and a PTFE lid which can fit the platinum counter electrode, the Ag/AgCl-reference electrode as well as the rotating working electrode positioned in the center of the cell.

The used electrochemical cell is also double walled and attached to an external heated water bath. During the experiments, water is pumped from this heated reservoir into the water jacket of the cell to control the water temperature within a 25°C to 35°C range.

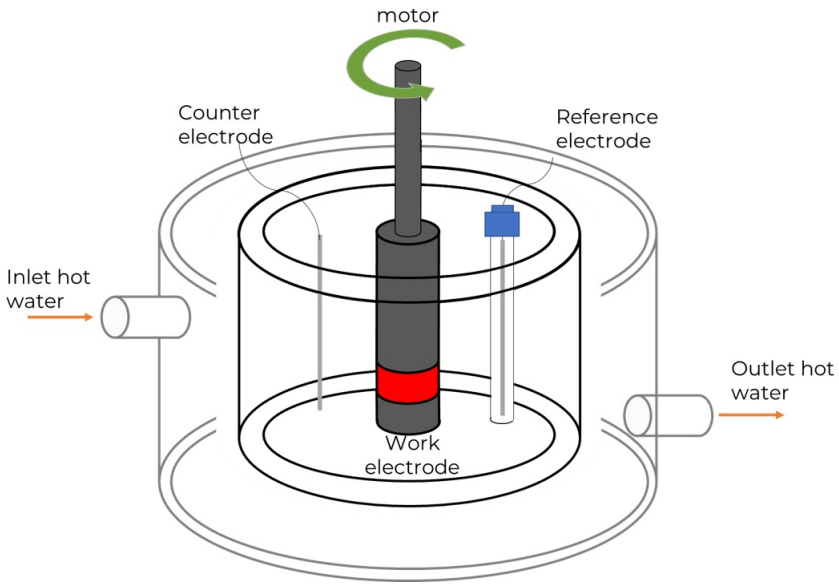

Figure 1: Schematic representation of Rotating cylinder electrode (RCE) cell setup

2.3 Potentiodynamic scan (PDS)

All electrochemical measurements are carried out utilizing a Gamry interface 1010 potentiostat, using a typical three-electrode system as described in section 2.2. A stable OCP is obtained after a period of approximately 4 hours, after which the PDS is started. The polarization curves are obtained by scanning a potential range between -0.5 V and 1.5 V with respect to the measured OCP at a scanning rate of 1 mV/s. [3,41] Each measurement was repeated twice to assure repeatability. Although no clear cathodic and anodic currents complying with a Tafel law can be identified, a Tafel extrapolation was done in order to give an approximation for relative corrosion speeds and potentials. In that respect, the corrosion potential (E_{corr}) and corrosion current density (J_{corr}) are acquired from the resulting Tafel plots at the intersection of the approximated anodic and cathodic Tafel lines determined at ±100 mV w.r.t. the measured E_{corr}. [42, 43] Based on this corrosion current density, an approximated inhibition efficiency can be defined as given in equation 1:

$$IE(\%) = \frac{J_{corr,0} - J_{corr,i}}{J_{corr,0}} \tag{1}$$

With $J_{corr,0}$ and $J_{corr,i}$ the corrosion current density of the uninhibited S235 steel and the S235 steel inhibited by SS, respectively.

2.4 Electrochemical impedance spectroscopy (EIS)

Impedance measurements are conducted to complement the PDS, as more information is obtained on the electrical properties of the complete electrochemical cell, and more specifically on the film properties and mechanism of film formation. Especially for inhibitors

acting on the metal surface, EIS can reveal extra information on charge transfer resistance and give a better overall estimation on the inhibition efficiency than polarization resistance measurements. [44] Furthermore, interfacial capacitance values can offer additional proof on the inhibition mode. [44]
EIS spectra are measured within the electrochemical cell described in section 2.2 after a 4 hour duration in order to obtain a stable OCP. The EIS experiments themselves are carried out starting at the measured OCP under potentiostatic regulation. Here, the electrochemical system is excited within the frequency range of 10kHz to 10mHz with 8 points per decade by applying a 10 mV_{rms} sinusoidal voltage with respect to the OCP. To validate stability, causality and linearity within the tested conditions, Kramers-Kronig relations are checked after each EIS measurement. For fitting the EIS data, the equivalent circuits in Figure 2 are used. This circuits consist of a typical Randles circuit, modified to account for two time-constants. For the circuit given in figure 2 b), an additional Warburg impedance Z_{dif} is included to account for diffusion. In these models, R_s, R_f and R_{ct} are resistances which correspond with the solution-, film- and charge transfer resistance, respectively. CPE_f and CPE_{dl} represent the film- and double layer capacitance, respectively, however constant phase elements (CPE) are used instead of ideal capacitors. The impedance of such a CPE is given by equation 2:

$$Z_{CPE} = \frac{1}{(j\omega)^{\alpha} Q} \tag{2}$$

With ω the frequency (Hz), Q the capacitance ($s^{\alpha}\Omega^{-1}m^{-2}$) and α an exponent related to the inhomogeneity of the electrode surface [3, 41]. In this study, both film- and double layer CPE's are identified, with corresponding film- (Q_f and α_f) and double layer (Q_{dl} and α_{dl}) capacitances and exponents. α can take a value of 0.5 for diffusion controlled processes and a value of 1 for ideal capacitors. In this way, the CPE is a fluid element between a resistive (real impedance) and a capacitive element (imaginary impedance). Based on the fitted charge transfer resistance, an inhibition efficiency can be defined according to equation 3:

$$IE(\%) = \frac{R_{ct,i} - R_{ct,0}}{R_{ct,i}} \tag{3}$$

With $R_{ct,0}$ and $R_{ct,i}$ the charge transfer resistances of the uninhibited S235 steel and the S235 steel inhibited by SS, respectively.

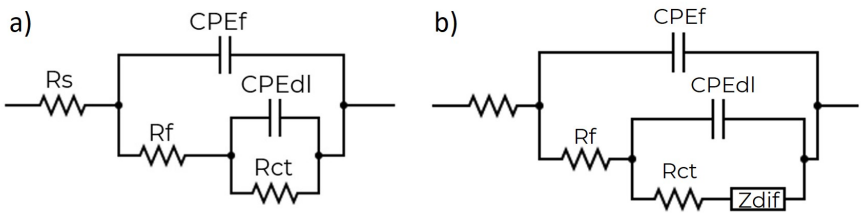

Figure 2: Equivalent circuits proposed to fit the EIS spectra obtained for S235 steel subjected to a dynamic salt water environment, with additional sodium silicate added as a corrosion inhibitor. a) with a low sodium silicate concentration; b) with 20 mM sodium silicate

2.5 Surface characterization

To characterize the composition of the formed protective film, XPS measurements were conducted post-immersion in a 3 wt.% NaCl salt water environment treated with 10 mM SS. During this 24 h immersion of the S235 steel ring , a constant temperature of 25°C and a constant RCE surface rotation speed of 0.5 m/s were maintained. The surface chemical composition was analysed using a PHI 5000 Versaprobe II spectrometer. The outer surface of the tested RCE-ring was excited with a monochromatic Al K_α X-ray source (hv=1486.6 eV) with a spot diameter of 100µm. The elements present in the film were quantified from the XPS spectra using Multipak software, which was also used for curve peak fitting of the high-resolution peak spectra.

3 Results

3.1 Potentiodynamic polarization

The polarization curves for S235 steel immersed in salt water solution with a varying sodium silicate (SS) concentration are given in Figure 3. As mentioned in section 2.1, SS is varied between a concentration of 0.1 mM and 20 mM SS within a 3 wt.% NaCl solution. This is done at a constant temperature of 25°C and while maintaining constant working electrode rotation speed of 0.5 m/s at the sample surface in order to investigate the effect of increased SS dosage in this dynamic regime. The determined corrosion current density (J_{corr}) and corrosion potential (E_{corr}) values for these PDS tests are given in Table 2. Here, a decreasing trend in J_{corr} is observed with increased silicate dosage, reaching a minimum value at a dosage of 0.01 mol/L SS in the considered dynamic environment. The decreasing trend in current density with increased SS concentration is also reflected in the increasing inhibition efficiency (Table 2). However, as mentioned in section 2.3, the absolute values should be interpreted as an approximation. Furthermore, a more cathodic corrosion potential is observed in the silicate-treated samples as compared to the reference test. With added sodium silicate, steeper cathodic and anodic curves were observed. This behaviour changes at 5 mM silicate where the anodic slope increases again, which is related to a current plateau starting to manifest itself at this concentration (anodic branches in Figure 3). This passive-like behaviour is possibly caused by a continuous, protective silicate layer being formed on the steel surface.

To assess the effect of temperature on the corrosion inhibition provided by silicate, PDS is done at 25, 30 and 35°C at a constant concentration of 0.5 mM SS and a constant flow rate of 0.5 m/s rotation speed at the working electrode surface. The determined J_{corr} and E_{corr}, as well as the calculated IE values for the PDS tests conducted with varying temperature are given in Table 3. From these results, it is observed that SS addition still results in a reduction in corrosion current density, although to a lower extent compared to at lower temperatures. This increase in corrosion current density is accompanied by a decrease in corrosion potential to a more negative value. Additionally, there is also a noticeable increasing trend in the anodic and cathodic slope, becoming slightly less steep.

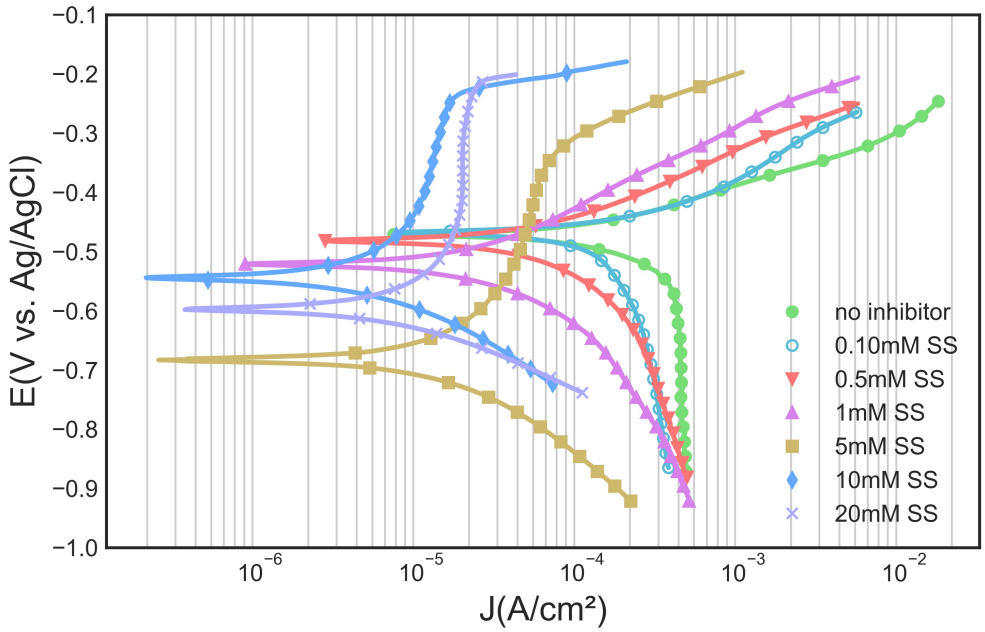

Figure 3: Polarization curves for S235 steel within 3 wt.% NaCl solution with SS inhibitor added in dosages varying from 0.1 to 20 mM; T: 25°C; surface rotation speed of 0.5 m/s

Table 2: Tafel-analysis parameters for PDS scans conducted on S235 steel in a 3 wt.% NaCl solution with a varied sodium silicate (SS) concentration; inhibition efficiency (IE) calculated based on corrosion current density (J_{corr}) w.r.t. the test with bare S235; rotation speed: 0.5 m/s at sample surface; β_a and β_c respectively anodic- and cathodic Tafel slope.

$SS(mM)$	$E_{corr}(Vvs.Ag/AgCl)$	$J_{corr}(mA/cm^2)$	$\beta_a(V/dec.)$	$\beta_c(V/dec.)$	$IE(\%)$
0	-0.430	0.258	0.078	0.894	-
0.1	-0.495	0.184	0.141	0.527	28.74%
0.5	-0.477	0.051	0.130	0.247	80.39%
1	-0.491	0.025	0.142	0.198	90.44%
5	-0.710	0.011	0.291	0.163	95.87%
10	-0.526	0.004	0.341	0.166	98.61%
20	-0.623	0.011	0.296	0.131	95.73%

Table 3: Tafel-analysis parameters for PDS scans conducted on S235 steel in a 3 wt.% NaCl solution and 0.5 mM sodium silicate (SS) with a varied temperature; inhibition efficiency (IE) calculated based on corrosion current density (J_{corr}) w.r.t. the test with bare S235 at 25°C; rotation speed: 0.5 m/s at sample surface; β_a and β_c respectively anodic- and cathodic Tafel slope.

$SS(mM)$	$T(°C)$	$E_{corr}(Vvs.Ag/AgCl)$	$J_{corr}(mA/cm^2)$	$\beta_a(V/dec.)$	$\beta_c(V/dec.)$	$IE(\%)$
0	25	-0.430	0.258	0.078	0.894	-
0.5	25	-0.477	0.051	0.130	0.247	80.39%
0.5	30	-0.488	0.083	0.124	0.316	67.71%
0.5	35	-0.503	0.115	0.161	0.324	55.49%

3.2 Electrochemical Impedance Spectroscopy

Impedance spectra are obtained for steel submerged in a salt water environment with an added SS concentration ranging from 0.1 mM to 20 mM SS. Tests are conducted at a constant cell temperature of 25°C with a constant working electrode rotation speed of

0.5 m/s. These conditions align with those used in the PDS measurements to validate trends in corrosion inhibition in this dynamic regime as well as to obtain additional information on the electrical properties of the electrochemical system (among which the resistive properties of the inhibited steel surface). The impedance spectra for S235 steel immersed in salt water solution with a varying sodium silicate concentration are given in Figure 4, with the fitted EIS parameters given in Table 4 and calculated pseudo-capacitance values according to Brug's Formula (C_{dl}) [45] and Hsu and Manfeld (C_f) [46] given in Table 5. The equivalent circuits were already given in Figure 2 and are used to fit and evaluate the measured impedance spectra. Here an inhibition efficiency is approximated based on the fitted charge transfer resistance value and also included in Table 4.

Table 4: EIS fitted parameters for EIS scans conducted on S235 steel in a 3 wt.% NaCl solution and a varied sodium silicate (SS) concentration; inhibition efficiency (IE) calculated based on the charge transfer resistance (R_{ct}) w.r.t. the test with bare S235; surface rotation speed (v_s): 0.5m/s; T: 25°C

$SS(mM)$	$R_s(\Omega)$	$R_f(\Omega)$	$R_{ct}(\Omega)$	$Q_f(\frac{ms^\alpha}{\Omega cm^2})$	$Q_{dl}(\frac{ms^\alpha}{\Omega cm^2})$	$\alpha_f(-)$	$\alpha_{dl}(-)$	$W(\frac{k\Omega}{\sqrt{s}})$	$IE(\%)$
0	10.72	3.41	95.74	0.39	1.70	1.00	0.78	-	-
0.1	11.54	47.41	172.92	3.18	6.34	0.58	0.69	-	44.63%
0.5	9.58	164.85	908.08	0.58	1.51	0.77	0.65	-	89.46%
1	10.57	575.13	2046.04	1.14	1.40	0.65	0.77	-	95.32%
5	11.21	467.15	22633.83	1.08	0.78	0.60	0.74	-	99.58%
10	10.83	1806.77	43790.10	0.88	0.29	0.68	0.90	-	99.78%
20	10.32	161.48	35350.20	0.15	0.38	0.82	0.82	16.77	99.56%

Looking at the EIS spectra in Figure 4, the measured Nyquist diagrams (Figure 4 a) consist of a capacitive loop, which can be split up into two capacitive contributions. This is better seen in the phase-angle plot (Bode plot: Figure 4 b), showing two separated phase noses, indicating that inhibition is not caused by geometric blocking. [44] In the fitted parameters (Table 4), a near constant solution resistance is noticed, which could be expected as only little variation (small SS dose) is imposed on the well-conducting salt water solution. On the other hand, an increase in charge transfer resistance is observed, as well as an overall increasing trend in the film resistance. This indicates that the SS treated metal surface is a more insulating one, and therefore provides a better protection against corrosion. This observation is also reflected in the resulting inhibition efficiencies (Table 4), also following this trend. At higher concentrations, a maximal IE is observed at a concentration of 10 mM, which is in line with the results obtained from the PDS tests (Figure 3). Furthermore, at a concentration of 20 mM SS, an additional influence of diffusion was observed, which is accounted for with the extra diffusion impedance (W), represented in the equivalent circuit of Figure 2 b.

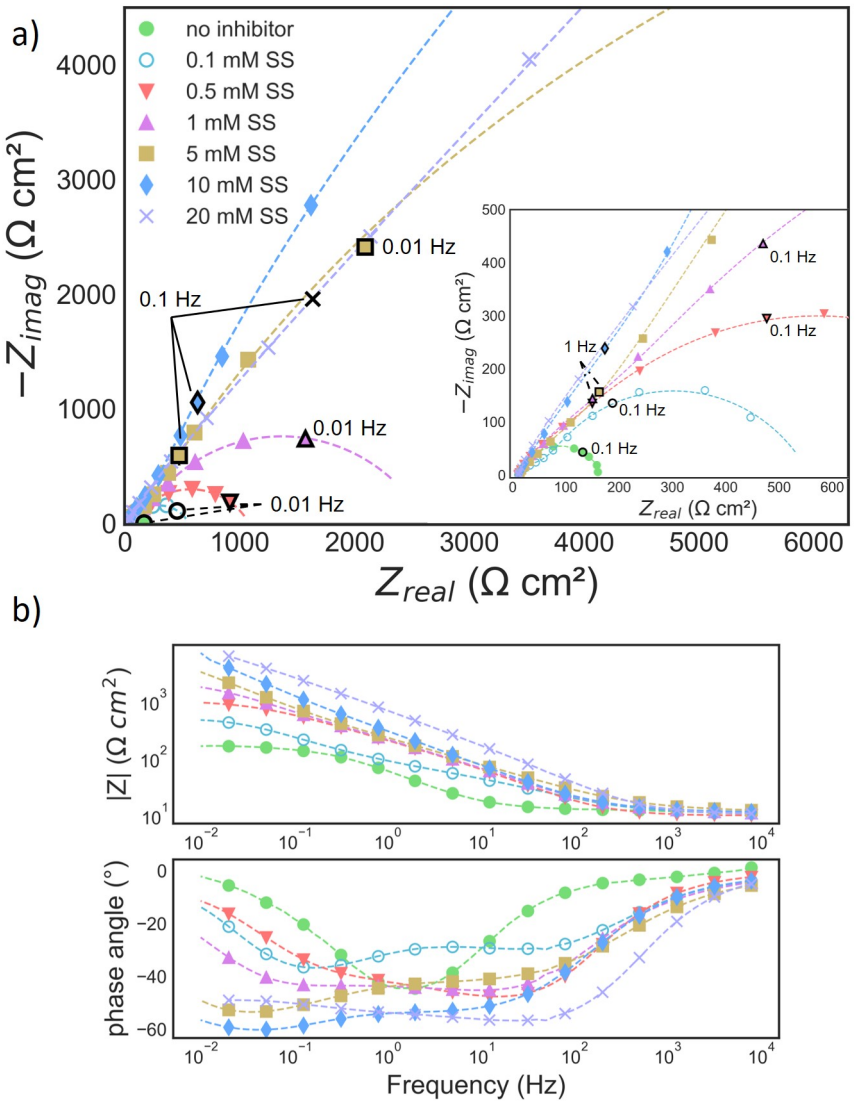

Figure 4: EIS Nyquist (a) and Bode (b) plot for S235 steel within 3 wt.% NaCl solution with varied SS inhibitor added; T:25°C; surface rotation speed: 0.5 m/s.

Table 5: Calculated double layer capacitance (C_{dl}) and film capacitance (C_f) for the respective CPE-element values Q_{dl} and Q_f given in Table 4

$SS(mM)$	$C_f(\frac{mF}{cm^2})$	$C_{dl}(\frac{mF}{cm^2})$
0	0.22	2.46
0.1	0.83	2.76
0.5	0.29	0.33
1	0.90	0.69
5	0.68	0.27
10	1.09	0.19
20	0.065	0.18

The fitted capacitive values Q_f and Q_{dl} given in Table 4 show a decrease, with the exception of the film capacitance for 0.5 mM SS, which is most likely related to the formation of the film on the steel surface from the silica in solution. This decreasing trend was also observed in the calculated quasi-capacitance values C_{dl} in table 5. This decreasing trend in capacity continues when increasing the SS concentration to 20 mM SS, although here

it should also be noted that a different equivalent circuit containing a diffusion element Z_{dif} (figure 2b) was used to fit the spectrum at the highest SS dose. As such, it is difficult to draw any conclusions in this regard. Looking at the exponents α_f and α_{dl}, no clear trend is observed. However, lower values are observed than compared to the bare steel surface, indicating less ideal capacitive behaviour. This fact is most-likely linked to the rougher surface, being a result of the formed film.

Apart from varying the inhibitor concentration in a dynamic regime, EIS measurements are also performed at different rotation speeds: 0.5, 0.625, 0.75, 0.875 and 1 m/s at the electrode surface. Temperature and dosage were kept constant (i.e. 0.5 mM SS at 25°C) in order to evaluate the effect of flow rate on the inhibition behaviour of SS. Figure 5 shows the resulting corresponding EIS spectra. For these measurements, the equivalent circuit of Figure 2a) is used to represent the electrochemical system. The fitted parameters are given in Table 6 with calculated pseudo-capacitance values according to Brug's Formula (C_{dl}) [45] and Hsu and Manfeld (C_f) [46] given in Table 7.

Table 6: EIS fitted parameters for EIS scans conducted on S235 steel in a 3 wt.% NaCl solution and 0.5mM sodium silicate (SS) with a varied flow speed; inhibition efficiency (IE) calculated based on the charge transfer resistance (R_{ct}) w.r.t. the test with bare S235; T: 25°C

$SS(mM)$	$v_s(m/s)$	$R_s(\Omega)$	$R_f(\Omega)$	$R_{ct}(\Omega)$	$Q_f(\frac{ms^\alpha}{\Omega cm^2})$	$Q_{dl}(\frac{ms^\alpha}{\Omega cm^2})$	$\alpha_f(-)$	$\alpha_{dl}(-)$	$IE(\%)$
0	0.5	10.72	3.41	95.74	0.39	1.70	1.00	0.78	-
0.5	0.5	9.58	164.85	908.08	0.58	1.51	0.77	0.65	89.46%
0.5	0.625	10.40	1.62	1316.66	0.37	1.09	0.80	0.50	92.73%
0.5	0.75	13.57	169.94	1649.48	0.49	1.42	0.78	0.55	94.20%
0.5	0.875	11.04	252.28	1321.78	1.03	2.00	0.66	0.65	92.76%
0.5	1	10.84	8.81	1058.04	1.10	0.04	0.57	0.97	90.95%

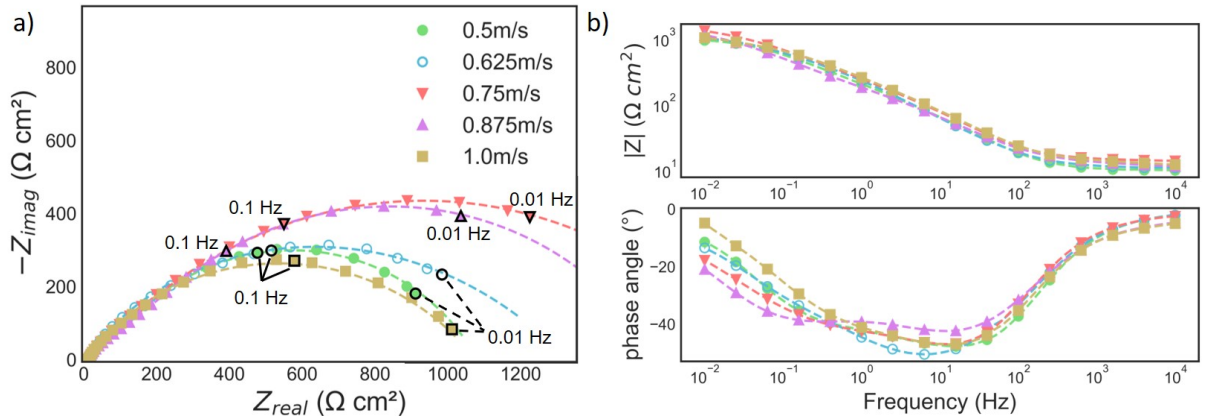

Figure 5: EIS Nyquist (a) and Bode (b) plot for S235 steel within 3 wt.% NaCl solution with 0.5 mM SS inhibitor added; T:25°C; surface rotation speed varied between 0.5 m/s and 1 m/s.

Table 7: Calculated double layer capacitance (C_{dl}) and film capacitance (C_f) for the respective CPE-element values Q_{dl} and Q_f given in Table 6

$v_s(m/s)$	$C_f(\frac{mF}{cm^2})$	$C_{dl}(\frac{mF}{cm^2})$
0.5	0.29	0.33
0.625	0.06	0.04
0.75	0.24	0.17
0.875	0.52	0.60
1	0.03	0.03

It is observed that with a higher rotation speed, the charge transfer resistance first increases, reaching a maximum value at 0.75 m/s. At rotation speeds exceeding 0.75 m/s, the R_{ct} decreased again in a similar fashion. This indicates that a more protective insulating layer is formed at intermediate flow rates. Here a couple of factors are playing: (1) the increase of flow rate accelerates the transfer of dissolved species (both agressive- and inhibitive), (2) the adsorption and desorption of silicate-species is influenced and (3) more mechanical removal of adsorbed species is possibly resulting from the higher flow rates.

To evaluate the stability of the formed inhibitor film, EIS measurements were performed after 1,5 and 10 days of immersion in a dynamic (v_s= 5 m/s) 3 wt.% NaCl environment treated with 10 mM SS. The impedance spectra are given in Figure 6, were fitted with the equivalent circuit given in Figure 2 a). The resulting fitted EIS-parameters are given in Table 8, with calculated pseudo-capacitance values according to Brug's Formula (C_{dl}) [45] and Hsu and Manfeld (C_f) [46] given in Table 9.

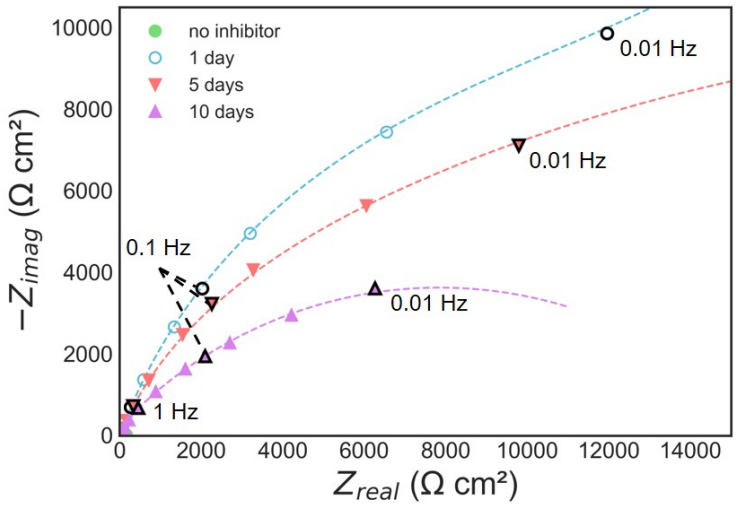

Figure 6: EIS Nyquist for S235 steel within 3 wt.% NaCl solution with 10 mM SS inhibitor added after 1,5 and 10 days of immersion; T:25°C; surface rotation speed: 0.5 m/s.

With increased immersion time, further little film development followed by slight film deterioration was observed. After one day, an increase is noticed in both film- and charge transfer resistances, as well as a significant decrease in film capacitance. With longer immersion, R_f and R_{ct} decrease again, resulting in a slight decrease of IE. Furthermore, both CPE's Q_f and Q_{dl} showed a slight decrease over time.

Table 8: EIS fitted parameters for EIS scans conducted on S235 steel in a 3 wt.% NaCl solution and 10 mM sodium silicate (SS) after different immersion times; inhibition efficiency (IE) calculated based on the charge transfer resistance (R_{ct}) w.r.t. the test with bare S235; T: 25°C

time(days)	$R_s(\Omega)$	$R_f(\Omega)$	$R_{ct}(\Omega)$	$Q_f(\frac{ms^\alpha}{\Omega cm^2})$	$Q_{dl}(\frac{ms^\alpha}{\Omega cm^2})$	$\alpha_f(-)$	$\alpha_{dl}(-)$	$IE(\%)$
1	8.47	20642.43	53026.80	0.32	0.57	0.78	0.52	99.82
5	8.56	10725.81	34900.20	0.30	0.39	0.77	0.50	99.73
10	8.69	1556.90	14467.14	0.23	0.34	0.79	0.50	99.34

Table 9: Calculated double layer capacitance (C_{dl}) and film capacitance (C_f) for the respective CPE-element values Q_{dl} and Q_f given in Table 8

time(days)	$C_f(\frac{mF}{cm^2})$	$C_{dl}(\frac{mF}{cm^2})$
1	0.54	0.011
5	0.43	0.004
10	0.17	0.003

3.3 Surface Characterization

As mentioned in section 2.5, XPS measurements were conducted on the S235 RCE-samples after immersion for 24 hours in a dynamic salt water environment with 10 mM SS added as corrosion inhibitor. High resolution XPS spectra were measured to investigate the surface chemistry of the deposited SS film. The spectra within the Si2p region and the O1s region are shown in figure 7 a) and b) respectively. Furthermore, over a complete spectrum survey, relative amounts of species were identified. In that respect, 65.3% of O, 23.5% of Si and 11.2% of C were obtained. Peaks related to other species (e.g. Fe, Cl, ...) remained under 1% and were as such not analysed further. In the Si2p region (figure 7a), the spectrum could be deconvoluted into 4 contributions of Si, with one peak being related to SiC at 102.36 eV and most contributions related to Si-O bonds in different Si to O ratios. These Si-O related contributions were seen in the peaks at 103.15 eV, 103.92 eV and 104.65 eV related to SiO, Si_2O_3 and SiO_2 respectively. [26, 47, 48] These Si-O bonds were also identified within the O1s spectrum region in figure 7 b) as Si-O-Si bonds at 532.66 eV [47, 48]. Other than that, a contribution of O-C at 531.24 eV and Si-OH at 533.36 eV were also found within the O1s region within the film spectrum. [26, 47, 48]

4 Discussion

The potentiodynamic scans represented in Figure 3 show good corrosion inhibition by adding sodium silicate, reaching a minimum in corrosion speed at 0.01 M silicate. A similar trend was observed in a previous study with simulated cooling water (SCW) in a static regime [16]. A passive zone is also observed at higher dosages ($\geq 5mM$), which is also observed in the sudden rise of the anodic Tafel-slope (β_a) in Table 2.

The impedance results obtained for SS given in Table 4 show a decrease in double layer capacitance from 6.37 $\frac{ms^\alpha}{\Omega cm^2}$ at 0.1 mM SS to 0.29 $\frac{ms^\alpha}{\Omega cm^2}$ at 10 mM SS. This decrease in Q_{dl} might be caused by a gradual replacement of water molecules by SS inhibitor molecules,

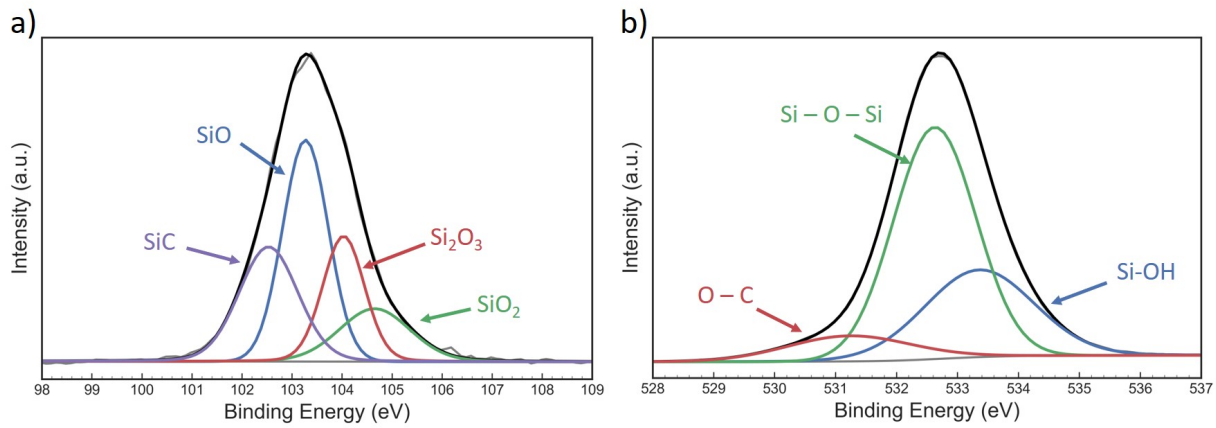

Figure 7: XPS spectra for a post-immersion RCE-sample surface a)Si2p binding energy region and b) O1s binding energy region

creating a protective film. The translation of the resulting film structure into the equivalent circuit given in Figure 2 is visualised in Figure 8. Furthermore, the double layer capacitance can be expressed as $C_{dl} = \epsilon\epsilon_0 S/d$ (with ϵ and ϵ_0 the relative dielectric constant and the dielectric constant in vacuum, respectively, S is the area of the metal-film interface and d the thickness of the double layer) [7]. Two interfaces are created when a silicate film is formed: a metal-film interface and a film-solution interface. This also becomes apparent from the phase-angle bode-plot in Figure 4 b), expressing two phase noses around 50Hz and 0.01Hz. The low frequency (0.01Hz) phase nose corresponds with the double layer capacitance at the steel-film interface while the high frequency (50Hz) phase nose corresponds to the film capacitance at the film-solution interface. As the film develops with an increased SS concentration, this corresponds with both larger phase peaks (more negative phase angles) and a slight shift of the peaks to lower frequency. This peak shift is largely related to both the increase in R_f and R_{ct}, as well as the decrease in relative capacitance values Q_{dl}/Q_f. The observed further decrease in Q_{dl} is possibly a result of a densification of the film structure near the metal-film interface, a growth of the overall film thickness or a combination of both. Moreover, some previous studies propose that silicate inhibition required the presence of corrosion product [5,33]. This implies that the film structure would be different near the metal-film interface compared to the rest of the silicate film. An increased concentration of SS in solution could then be the reason for a denser, better attached network to be formed near the steel surface. This improved silicate network structure containing less overall point defects would then be responsible for a decreased ionic mobility and consequently a lowered double layer capacitance and an increased charge transfer resistance.

An explanation for the similar decreasing trend observed in the Q_f can again be found in the replacement of water molecules at the film-solution interface by silicate molecules. When the SS concentration is increased further from 10 mM SS to 20 mM SS in solution, the Q_{dl} again shows an increase, although it is difficult to compare these results due to the difference in equivalent circuit and as such an altered inhibition mechanism. A possible explanation, however, can be found by a difference in the aqueous sodium

silicate state [5, 11, 49]. Polymeric, insoluble silica and more likely monomeric silicic acid ($Si(OH)_4$) can be more present. In the performed tests this is also noticed as gel-like silicate remained as a residue within the electrochemical test cell. On the other hand, the increased concentration of silicate in solution can increase film growth and the resulting film-thickness, explaining the better fit with an equivalent circuit utilizing a diffusion element Z_{dif}.
Regarding the charge transfer- and film resistances, an increasing trend is noticed with increasing SS concentration. As stated before, the formation of a more structured (i.e. less point defects), better adsorbed silicate network to the steel surface could decrease the ionic mobility within the film, increasing R_{ct}. This formed silicate film is most likely a complex structure, with an iron-oxide-silicate base near the steel surface. As discussed in section 3.3 the presence of this silicate film was also confirmed and characterized. Moreover, the Si in the formed film also appeared under different oxidation states (SiO, Si_2O_3, SiO_2 and Si-OH), indicating the complex formed network near the film-steel interface. Additionally, the obtained surface chemistry also indicates the absence of Fe near the film-solution interface.

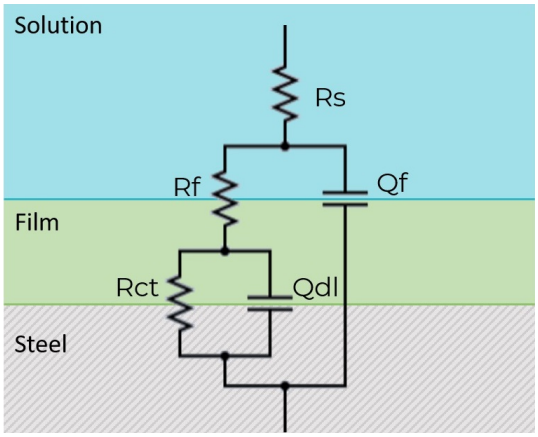

Figure 8: Schematic representation of the proposed equivalent circuit with the studied electrochemical system

When immersing the sample for longer duration, first an increase was was observed in R_f and R_{ct} after one day, related to slight further film (and interface) development, followed by a decrease over longer periods of time. These changes in interface resistances is also noticed in the change of IE, showing a very slight increase to 99.82%, followed by a slight decrease over time to 99.34% after 10 days. For further practical use, this degradation in film properties over time could possibly be circumvented by continuous dosage of SS. [19]

Regarding the effect of temperature and flow rate, previous works [11, 19, 30] indicated that the protection of silicate in aqueous systems is both worse in static systems and at higher temperatures. This deterioration in corrosion protection at higher temperatures is also noticed in the PDS tests within a dynamic flow regime (Table 3), and is most likely related to faster desorption kinetics as well as less stable bonding between the film and the steel surface at these temperatures. Concerning the effect of flow rate, the most protective film is formed at an intermediate flow rate of 0.75 m/s surface rotation speed.

(Figure 5). A possible explanation for this behaviour lies in an optimal balance between a faster transportation of bulk species to the steel surface as well as hydrodynamic flow effects at higher flow rates. Assuming a uniform concentration profile of species (as the solution is well-mixed before testing), at lower flow rates the transport of silicate species to the steel surface is most likely insufficient to deal with the high dissolved chlorine- and oxygen concentrations. With an increasing flow rate, the diffusion boundary layer thickness decreases, implying a faster delivery of silicate from the bulk to the sample and a better possibility to form a less permeable film. [27]

5 Conclusion

The present study evaluated the corrosion behaviour of S235 carbon steel inhibited by sodium silicate (SS) in a dynamic 3 wt.% NaCl environment. For this, electrochemical measurements (PDS and EIS) were performed within a rotating cylinder electrode (RCE) setup. $Na_2Si_3O_7$ showed good inhibitive properties, showing similar trends in both EIS and PDS measurements. Decreasing corrosion current densities (in PDS) and increasing charge transfer resistance values (in EIS) were measured upon increasing the SS concentration, reaching a maximum inhibition efficiency (IE) of 98.61% and 99.78% for PDS and EIS, respectively, at 10 mM SS in solution.
Furthermore, EIS revealed characteristics of the film's electrical properties at different SS doses. A possible film formation mechanism was proposed to consist of first replacing water molecules at the steel-solution interface (with silicate being adsorbed to the metal surface), resulting in a decreasing film capacitance. This step would then be complemented by a more structured film formation, resulting in the reduction of film defects and thus a decrease in ionic mobility through the film. The formation of this protective silicate film at the steel surface was confirmed by performing XPS analysis. Here, it was apparent that the outer film composition was mainly the proposed SiOx network, with Si being present in several different oxidation states. When immersed for longer times in the dynamic regime, slight degradation of the film properties was observed with EIS over a period of 10 days.
Increasing the solution temperature in the dynamic regime resulted in a decrease of IE for 0.5 mM SS, which is possibly related to faster reaction kinetics and change in film stability at these higher temperatures.
Faster flow rates resulted in a higher IE at a constant SS dose of 0.5 mM, reaching a maximum of 94.20% at 0.75 m/s surface rotation speed. This behaviour can be explained by a balance between mechanical removal of film and a faster transfer of inhibiting SS species and cathodic species to the metal surface upon increasing the flow rate.

Acknowledgements

The authors would like to thank the senior postdoctoral fellowship of the Research Foundation –Flanders (FWO) via grant 12ZO420N and the Special Research Fund (BOF),

UGent (grants BOF/GOA/026) for support.

Data availability

The raw/processed data required to reproduce these findings cannot be shared at this time as the data also forms part of an ongoing study.

References

[1] W. Faes, S. Lecompte, Z. Y. Ahmed, J. V. Bael, R. Salenbien, K. Verbeken, and M. D. Paepe, "Corrosion and corrosion prevention in heat exchangers," *Corrosion Reviews*, vol. 37, pp. 131–155, 4 2019.

[2] C. Verma, E. E. Ebenso, and M. A. Quraishi, "Corrosion inhibitors for ferrous and non-ferrous metals and alloys in ionic sodium chloride solutions: A review," *Journal of Molecular Liquids*, vol. 248, pp. 927–942, 12 2017.

[3] B. Zhang, C. He, X. Chen, Z. Tian, and F. Li, "The synergistic effect of polyamidoamine dendrimers and sodium silicate on the corrosion of carbon steel in soft water," *Corrosion Science*, vol. 90, pp. 585–596, 1 2015.

[4] Z. Sanaei, T. Shahrabi, and B. Ramezanzadeh, "Synthesis and characterization of an effective green corrosion inhibitive hybrid pigment based on zinc acetate-cichorium intybus l leaves extract (zna-cil.l): Electrochemical investigations on the synergistic corrosion inhibition of mild steel in aqueous chloride solutions," *Dyes and Pigments*, vol. 139, pp. 218–232, 4 2017.

[5] M. Salasi, T. Shahrabi, E. Roayaei, and M. Aliofkhazraei, "The electrochemical behaviour of environment-friendly inhibitors of silicate and phosphonate in corrosion control of carbon steel in soft water media," *Materials Chemistry and Physics*, vol. 104, pp. 183–190, 7 2007.

[6] R. Touir, N. Dkhireche, M. E. Touhami, M. Lakhrissi, B. Lakhrissi, and M. Sfaira, "Corrosion and scale processes and their inhibition in simulated cooling water systems by monosaccharides derivatives: Part i: Eis study," *Desalination*, vol. 249, pp. 922–928, 12 2009.

[7] R. Touir, N. Dkhireche, M. E. Touhami, M. Sfaira, O. Senhaji, J. J. Robin, B. Boutevin, and M. Cherkaoui, "Study of phosphonate addition and hydrodynamic conditions on ordinary steel corrosion inhibition in simulated cooling water," *Materials Chemistry and Physics*, vol. 122, pp. 1–9, 7 2010.

[8] G. Serdaroğlu, S. Kaya, and R. Touir, "Eco-friendly sodium gluconate and trisodium citrate inhibitors for low carbon steel in simulated cooling water system: Theoretical study and molecular dynamic simulations," *Journal of Molecular Liquids*, vol. 319, p. 114108, 12 2020.

[9] S. A. Umoren and M. M. Solomon, "Synergistic corrosion inhibition effect of metal cations and mixtures of organic compounds: A review," *Journal of Environmental Chemical Engineering*, vol. 5, pp. 246–273, 2 2017.

[10] H. H. Ou, Q. T. P. Tran, and P. H. Lin, "A synergistic effect between gluconate and molybdate on corrosion inhibition of recirculating cooling water systems," *Corrosion Science*, vol. 133, pp. 231–239, 4 2018.

[11] N. Asrar, A. U. Malik, and S. Ahmed, "Corrosion prevention with sodium silicate," Saline Water Conversion Corporation, Tech. Rep., 7 1998.

[12] J. Baux, N. Caussé, S. Delaunay, J. Tireau, M. Roy, D. You, and N. Pébère, "Film-forming amines for the corrosion protection of carbon steels in nuclear power plant secondary circuit conditions: An impedance study," *Journal of The Electrochemical Society*, vol. 167, no. 6, p. 061504, 3 2020.

[13] I. Betova, M. Bojinov, and T. Saario, "Film-forming amines in steam/water cycles–structure, properties, and influence on corrosion and deposition processes," Technical Research Centre of Finland (VTT), Tech. Rep., 7 2014.

[14] Y. Chen, W. Xing, L. Wang, and L. Chen, "Experimental and electrochemical research of an efficient corrosion and scale inhibitor," *Materials*, vol. 12, p. 27242, 11 2019.

[15] R. D. Armstrong, L. Peggs, and A. Walsh, "Behaviour of sodium silicate and sodium phosphate (tribasic) as corrosion inhibitors for iron," *Journal of Applied Electrochemistry*, vol. 24, pp. 1244–1248, 12 1994.

[16] R. A. Anaee, "Sodium silicate and phosphate as corrosion inhibitors for mild steel in simulated cooling water system," *Arabian Journal for Science and Engineering*, vol. 39, pp. 153–162, 11 2014.

[17] R. Touir, N. Dkhireche, M. E. Touhami, M. E. Bakri, A. H. Rochdi, and R. A. Belakhmima, "Study of the mechanism action of sodium gluconate used for the protection of scale and corrosion in cooling water system," *Journal of Saudi Chemical Society*, vol. 18, pp. 873–881, 12 2014.

[18] M. R. Yuan, J. T. Lu, G. Kong, and C. S. Che, "Effect of silicate anion distribution in sodium silicate solution on silicate conversion coatings of hot-dip galvanized steels," *Surface and Coatings Technology*, vol. 205, pp. 4466–4470, 6 2011.

[19] J. L. Thompson, B. E. Scheetz, M. R. Schock, D. A. Lytle, and P. J. Delaney, "Sodium silicate corrosion inhibitors: Issues of effectiveness and mechanism," PQ Corporation, Tech. Rep., 11 1997.

[20] J.-R. Chen, H.-Y. Chao, Y.-L. Lin, I.-J. Yang, J.-C. Oung, and F.-M. Pan, "Studies on carbon steel corrosion in molybdate and silicate solutions as corrosion inhibitors," *Surface Science*, vol. 247, pp. 352–359, 5 1991.

[21] J. W. Wood, J. S. Beecher, and P. S. Laurence, "Some experiences with sodium silicate as a corrosion inhibitor in industrial cooling waters," *Corrosion*, vol. 13, pp. 41–46, 11 1957.

[22] R. D. Armstrong and S. Zhou, "The corrosion inhibition of iron by silicate related materials," *Corrosion Science*, vol. 28, pp. 1177–1181, 1 1988.

[23] E. P. Katsanis, W. D. Esmonde, and R. W. Spencer, "Soluble silicate corrosion inhibitors in water systems," *Materials Performance*, vol. 25, pp. 19–25, 5 1986.

[24] D. A. Awizar, N. K. Othman, A. Jalar, A. R. Daud, I. A. Rahman, and N. H. Al-Hardan, "Nanosilicate extraction from rice husk ash as green corrosion inhibitor," *International Journal of Electrochemical Science*, vol. 8, pp. 1759–1769, 2 2013.

[25] J. Zhao, M. Zhang, and Z. Tie, "Synergistic inhibition effect of sodium silicate and acrylamide on the corrosion of carbon steel in a high-concentration kcl solution," *Chemical Research in Chinese Universities*, vol. 33, pp. 100–106, 1 2017.

[26] L. A. de Oliveira, O. V. Correa, D. J. dos Santos, A. A. Z. Páez, M. C. L. de Oliveira, and R. A. Antunes, "Effect of silicate-based films on the corrosion behavior of the api 5l x80 pipeline steel," *Corrosion Science*, vol. 139, pp. 21–34, 7 2018.

[27] C. Wang, J. Chen, B. Hu, Z. Liu, C. Wang, J. Han, M. Su, Y. Li, and C. Li, "Modified chitosan-oligosaccharide and sodium silicate as efficient sustainable inhibitor for carbon steel against chloride-induced corrosion," *Journal of Cleaner Production*, vol. 238, p. 117823, 11 2019.

[28] S. W. Osterhus, "The effect of mineralization and silicate addition for corrosion control in soft low carbonate waters," *Water Science and Technology: Water Supply*, vol. 1, pp. 59–73, 6 2001.

[29] M. Salasi, T. Shahrabi, and E. Roayaei, "Effect of inhibitor concentration and hydrodynamic conditions on the inhibitive behaviour of combinations of sodium silicate and hedp for corrosion control in carbon steel water transmission pipes," *Anti-Corrosion Methods and Materials*, vol. 54, pp. 82–92, 3 2007.

[30] M. E. Mohorich, J. Lamb, D. Chandra, J. Daemen, and R. B. Rebak, "Electrochemical studies on silicate and bicarbonate ions for corrosion inhibitors," *Metallurgical and Materials Transactions A: Physical Metallurgy and Materials Science*, vol. 41, pp. 2563–2574, 6 2010.

[31] H. Gao, Q. Li, F. N. Chen, Y. Dai, F. Luo, and L. Q. Li, "Study of the corrosion inhibition effect of sodium silicate on az91d magnesium alloy," *Corrosion Science*, vol. 53, pp. 1401–1407, 4 2011.

[32] K. Aramaki, "Self-healing mechanism of an organosiloxane polymer film containing sodium silicate and cerium(iii) nitrate for corrosion of scratched zinc surface in 0.5 m nacl," *Corrosion Science*, vol. 44, pp. 1621–1632, 7 2002.

[33] V. S. Saji and S. M. Shibli, "Synergistic inhibition of carbon steel corrosion by sodium tungstate and sodium silicate in neutral aqueous media," *Anti-Corrosion Methods and Materials*, vol. 49, pp. 433–443, 12 2002.

[34] W. Stericker, "Protection of small water systems from corrosion." *Industrial Engineering Chemistry*, vol. 37, pp. 716–720, 8 1945.

[35] G. S. Vasyliev, "The influence of flow rate on corrosion of mild steel in hot tap water," *Corrosion Science*, vol. 98, pp. 33–39, 9 2015.

[36] R. A. Pisigan and J. E. Singley, "Influence of buffer capacity, chlorine residual, and flow rate on corrosion of mild steel and copper," *Journal - American Water Works Association*, vol. 79, pp. 62–70, 2 1987.

[37] N. Ochoa, F. Moran, N. Pébère, and B. Tribollet, "Influence of flow on the corrosion inhibition of carbon steel by fatty amines in association with phosphonocarboxylic acid salts," *Corrosion Science*, vol. 47, pp. 593–604, 9 2005.

[38] S. Guo, J. J. Leavitt, X. Zhou, Y. Xie, S. Tietze, Y. Zhu, A. Lawver, E. Lahti, and J. Zhang, "Effects of flow, si inhibition, and concurrent corrosion of dissimilar metals on the corrosion of aluminium in the environment following a loss-of-coolant accident," *Corrosion Science*, vol. 128, pp. 100–109, 11 2017.

[39] H. L. Shuldener and S. Sussman, "Silicate as a corrosion inhibitor in water systems," *Corrosion*, vol. 16, pp. 354t–358t, 7 1960.

[40] J. C. Rushing, L. S. McNeill, and M. Edwards, "Some effects of aqueous silica on the corrosion of iron," *Water Research*, vol. 37, pp. 1080–1090, 3 2003.

[41] W. Zhang, H. J. Li, L. Chen, J. Sun, X. Ma, Y. Li, C. Liu, X. Han, B. Pang, and Y. C. Wu, "Performance and mechanism of a composite scaling–corrosion inhibitor used in seawater: 10-methylacridinium iodide and sodium citrate," *Desalination*, vol. 486, p. 114482, 7 2020.

[42] T. D. Seranno, E. Lambrechts, E. D. Meyer, W. Hater, N. D. Geyter, A. R. Verliefde, T. Depover, and K. Verbeken, "Effect of film-forming amines on the acidic stress-corrosion cracking resistance of steam turbine steel," *Metals*, vol. 10, pp. 1–20, 12 2020.

[43] T. D. Seranno, E. Lambrechts, A. R. Verliefde, T. Depover, and K. Verbeken, "Stress corrosion cracking of steam turbine steel: The influence of organic acid characteristics," *Metals*, vol. 12, p. 1490, 9 2022.

[44] C. Cao, "On electrochemical techniques for interface inhibitor research," *Corrosion Science*, vol. 38, pp. 2073–2082, 12 1996.

[45] G. J. Brug, A. L. van den Eeden, M. Sluyters-Rehbach, and J. H. Sluyters, "The analysis of electrode impedances complicated by the presence of a constant phase element," *Journal of Electroanalytical Chemistry*, vol. 176, pp. 275–295, 9 1984.

[46] C. H. Hsu and F. Mansfeld, "Technical note: Concerning the conversion of the constant phase element parameter y0 into a capacitance," *Corrosion*, vol. 57, pp. 747–748, 9 2001.

[47] J. W. Ma, W. J. Lee, J. M. Bae, K. S. Jeong, S. H. Oh, J. H. Kim, S. H. Kim, J. H. Seo, J. P. Ahn, H. Kim, and M. H. Cho, "Carrier mobility enhancement of tensile strained si and sige nanowires via surface defect engineering," *Nano Letters*, vol. 15, pp. 7204–7210, 11 2015.

[48] B. V. Crist, "Xps in industry—problems with binding energies in journals and binding energy databases," *Journal of Electron Spectroscopy and Related Phenomena*, vol. 231, pp. 75–87, 2 2019.

[49] L. Lunevich, "Aqueous silica and silica polymerisation," in *Desalination - Challenges and Opportunities*, M. H. D. A. Farahani, V. Vatanpour, and A. Taheri, Eds. IntechOpen, 3 2019, pp. 99–117.